Cell

The *Arabidopsis* Chromatin-Modifying Nuclear siRNA Pathway Involves a Nucleolar RNA Processing Center

Olga Pontes,[1] Carey Fei Li,[2] Pedro Costa Nunes,[1,4] Jeremy Haag,[1] Thomas Ream,[1] Alexa Vitins,[1] Steven E. Jacobsen,[2,3] and Craig S. Pikaard[1,*]
[1] Biology Department, Washington University, 1 Brookings Drive, St. Louis, MO 63130, USA
[2] Department of Molecular, Cell and Developmental Biology
[3] Howard Hughes Medical Institute
University of California, Los Angeles, Los Angeles, CA 90095, USA
[4] Secção de Genética, Centro de Botânica Aplicada à Agricultura, Instituto Superior de Agronomia, Tapada da Ajuda, 1349-017 Lisboa, Portugal
*Contact: pikaard@biology.wustl.edu
DOI 10.1016/j.cell.2006.05.031

SUMMARY

In *Arabidopsis thaliana*, small interfering RNAs (siRNAs) direct cytosine methylation at endogenous DNA repeats in a pathway involving two forms of nuclear RNA polymerase IV (Pol IVa and Pol IVb), RNA-DEPENDENT RNA POLYMERASE 2 (RDR2), DICER-LIKE 3 (DCL3), ARGONAUTE4 (AGO4), the chromatin remodeler DRD1, and the de novo cytosine methyltransferase DRM2. We show that RDR2, DCL3, AGO4, and NRPD1b (the largest subunit of Pol IVb) colocalize with siRNAs within the nucleolus. By contrast, Pol IVa and DRD1 are external to the nucleolus and colocalize with endogenous repeat loci. Mutation-induced loss of pathway proteins causes downstream proteins to mislocalize, revealing their order of action. Pol IVa acts first, and its localization is RNA dependent, suggesting an RNA template. We hypothesize that maintenance of the heterochromatic state involves locus-specific Pol IVa transcription followed by siRNA production and assembly of AGO4- and NRPD1b-containing silencing complexes within nucleolar processing centers.

INTRODUCTION

In diverse eukaryotes, small interfering RNAs (siRNAs) regulate processes that include mRNA degradation, viral suppression, centromere function, and silencing of retrotransposons and endogenous DNA repeats (Almeida and Allshire, 2005; Baulcombe, 2004; Grewal and Rice, 2004; Tomari and Zamore, 2005). siRNAs are generated by Dicer endonuclease cleavage of double-stranded RNAs (dsRNAs), whose production in *Neurospora*, *C. elegans*, *S. pombe*, and plants involves one or more RNA-dependent RNA polymerases (RdRPs) (Baulcombe, 2004; Wassenegger and Krczal, 2006). Following dicing of dsRNAs into ~20–25 bp duplexes (Bernstein et al., 2001; Hannon, 2002), one RNA strand is loaded into effector complexes that carry out the silencing functions. A defining feature of these effector complexes is the inclusion of an Argonaute (AGO) family protein (Carmell et al., 2002; Sontheimer and Carthew, 2004). In RNA-slicing effector complexes, the AGO-associated siRNA base pairs with its target, thereby positioning the target RNA for endonucleolytic cleavage (Song et al., 2004). Within effector complexes that direct chromatin modifications (Grewal and Rice, 2004; Verdel et al., 2004; Volpe et al., 2002; Wassenegger, 2005), the mechanisms by which siRNAs guide target modifications are not yet understood.

In *Arabidopsis thaliana,* silencing at endogenous repeat loci involves histone H3K9 methylation and RNA-directed DNA methylation that is correlated with the production of homologous siRNAs (Cao et al., 2003; Lippman et al., 2003; Xie et al., 2004; Zilberman et al., 2004). Key players in this chromatin-modifying nuclear siRNA pathway include DICER-LIKE 3 (DCL3), ARGONAUTE4 (AGO4), RNA-DEPENDENT RNA POLYMERASE 2 (RDR2), and two forms of nuclear RNA polymerase IV (Pol IV). The largest and second largest subunits of Pol IV are similar to the catalytic β and β′ subunits of *E. coli* DNA-dependent RNA polymerase and to the corresponding subunits of eukaryotic nuclear RNA polymerases I, II, and III (see Onodera et al., 2005 and references therein). Two genes encode distinct Pol IV largest subunits, and two genes encode Pol IV second largest subunits. Both of the largest-subunit genes (*NRPD1a* and *NRPD1b*) are expressed, but only one of the second-largest-subunit genes (*NRPD2a*) is functional (Herr et al., 2005; Onodera et al., 2005; Pontier et al., 2005). As a result, there are two genetically nonredundant forms of Pol IV, namely Pol IVa and Pol IVb,

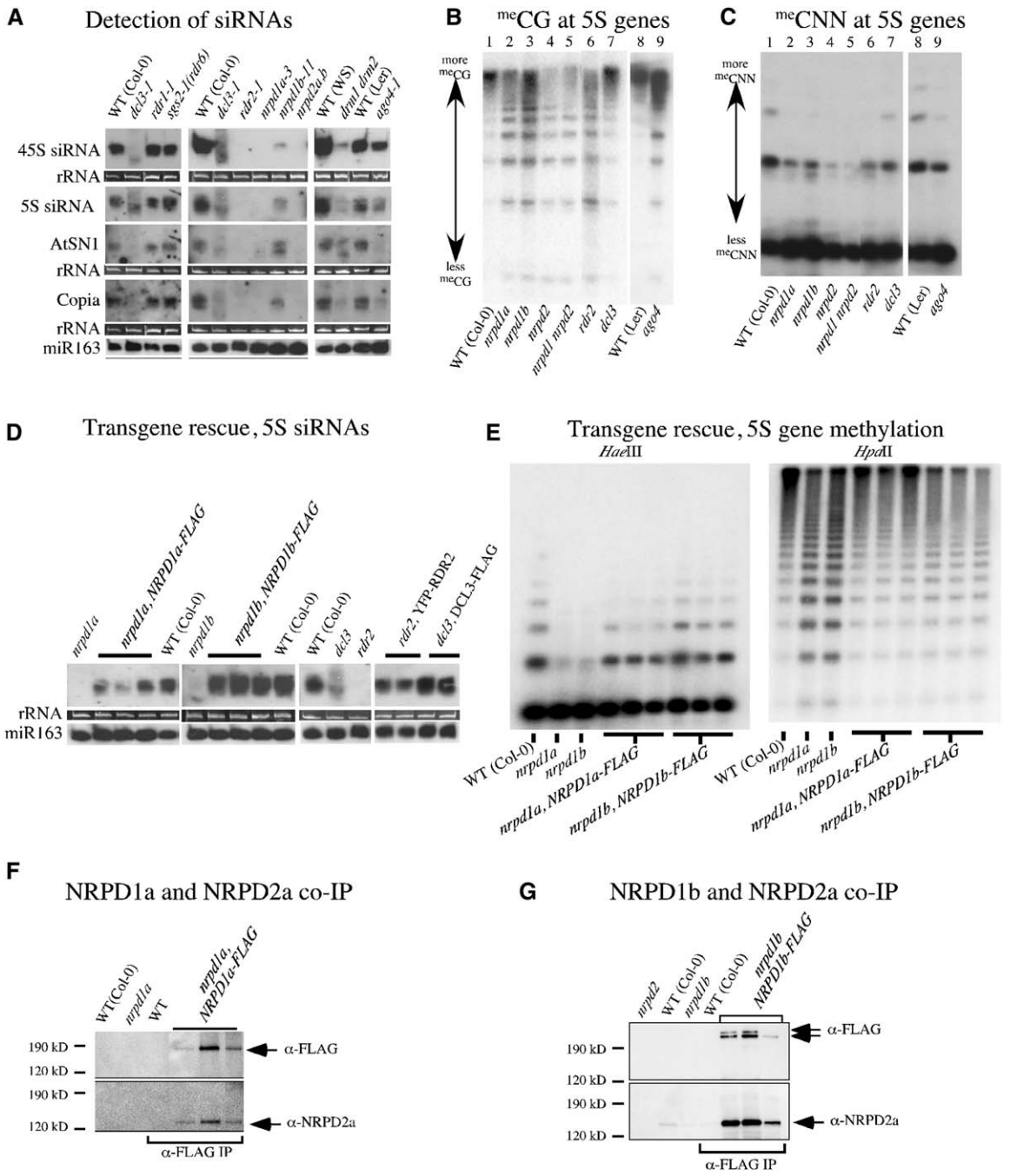

Figure 1. Loss of siRNAs and Cytosine Methylation at Repeated DNA Sequences in Mutants of the Nuclear siRNA Pathway

(A) siRNAs of wild-type (WT) and mutant plants. RNA blots were hybridized to probes corresponding to the 45S rRNA gene intergenic spacer (45S siRNA), the 5S rRNA gene siRNA siR1003, the *AtSN1* family of retroelements, the *Copia* transposable element family, or the microRNA miR163.

(B and C) Loss of CG or CNN methylation at 5S gene repeats. Genomic DNA digested with HpaII or HaeIII was hybridized to a 5S gene probe. *nrpd1a*, *nrpd1b*, *nrpd2*, *rdr2*, and *dcl3* mutants are in the Col-0 genetic background. *ago4* is in the Ler background.

(D) siRNA production in *nrpd1a*, *nrpd1b*, *rdr2*, and *dcl3* mutants is rescued by corresponding transgenes. Genomic clones under the control of their own promoters and encoding C-terminal FLAG-tagged proteins rescued the *nrpd1a*, *nrpd1b*, and *dcl3* mutants (three, three, and two independent transformants, respectively), whereas a YFP-RDR2 cDNA fusion under the control of the cauliflower mosaic virus 35S promoter rescued *rdr2* (two independent transformants shown).

(E) Transgene rescue of 5S rDNA methylation in *nrpd1a* and *nrpd1b* mutants. Southern blot analysis of HaeIII- and HpaII-digested genomic DNA with a 5S gene probe shows that the loss of methylation in *nrpd1a* and *nrpd1b* mutants, relative to wild-type (WT), is restored in each of three independent *NRPD1a-FLAG* or *NRPD1b-FLAG* transgenic lines.

designated according to which largest subunit is used. Disruption of Pol IV, RDR2, DCL3, or AGO4 genes causes decreased cytosine methylation and siRNA accumulation at endogenous repeats, including 5S ribosomal RNA genes and transposable elements (Herr et al., 2005; Kanno et al., 2005; Onodera et al., 2005; Pontier et al., 2005; Xie et al., 2004). However, the order in which these proteins act in the biogenesis of nuclear siRNAs is unclear.

Using RNA fluorescence in situ hybridization (RNA-FISH) together with protein immunolocalization, we present evidence for siRNA processing centers associated with the nucleolus. Within these centers, siRNAs colocalize with a significant portion of the RDR2, DCL3, AGO4, and NRPD1b protein pools. The two subunits of Pol IVa, however, do not localize to the processing centers but colocalize with chromosomal loci that are both sources and targets of siRNAs. A portion of the NRPD1b pool also colocalizes with target loci, as does the SWI2/SNF2 chromatin-remodeling ATPase family member DRD1, a protein required for RNA-directed DNA methylation that acts downstream of siRNA production (Kanno et al., 2004). Based on cytological, biochemical, and genetic evidence, we present a spatial and temporal model for nuclear siRNA biogenesis.

RESULTS

Loss of siRNAs and Cytosine Methylation in Nuclear siRNA Pathway Mutants

In *A. thaliana*, siRNAs homologous to repeated gene families are readily detected on RNA blots, as shown for siRNAs corresponding to the intergenic spacers of 45S or 5S rRNA genes or siRNAs corresponding to *AtSN1* or *Copia* transposable-element families (Figure 1A). Collectively, these endogenous repeats represent genes transcribed by RNA polymerase I (45S rRNA genes), RNA polymerase II (*Copia* elements), and RNA polymerase III (5S genes, *AtSN1* elements). The siRNAs are essentially eliminated upon mutation of the Pol IVa largest subunit, *NRPD1a*, or upon mutation of the second subunit of both Pol IVa and Pol IVb, *NRPD2* (note that the *nrpd2a-2 nrpd2b-1* double mutant [Onodera et al., 2005] is abbreviated as *nrpd2* throughout this paper). siRNAs are also eliminated in *rdr2* mutants. By contrast, siRNAs are reduced in abundance, but not eliminated, in *nrpd1b* or *ago4* mutants. A smear of alternatively sized small RNAs is generated in a *dcl3* mutant (Figure 1A) and is probably explained by the action of alternative Dicers (Gasciolli et al., 2005). The abundance of siRNAs is also greatly reduced in the *drm1 drm2* mutant, indicating that de novo cytosine methylation plays a role in nuclear siRNA accumulation.

Loss of endogenous siRNAs correlates with loss of cytosine methylation at corresponding DNA sequences. For instance, 5S gene repeats are heavily methylated at CG motifs, making them resistant to digestion by the methylation-sensitive restriction endonuclease HpaII in wild-type *A. thaliana* (Figure 1B, lanes 1 and 8). CG methylation at HpaII sites is decreased to a similar extent in *rdr2*, *ago4*, *nrpd1a*, *nrpd1b*, and *nrpd2* mutants, resulting in more hybridization signal in digested bands nearer the bottom of Southern blots (Figure 1B). Methylation is least affected in a *dcl3* mutant, presumably because other Dicers partially compensate (Gasciolli et al., 2005).

CNN methylation is a hallmark of RNA-directed DNA methylation, which is accomplished by the de novo cytosine methyltransferase DRM2 (Cao et al., 2003). At 5S gene loci, sensitivity to digestion by HaeIII reports on CNN methylation. 5S genes are more sensitive to HaeIII digestion in *rdr2*, *nrpd1a*, *nrpd1b*, and *nrpd2* mutants compared to wild-type plants (Figure 1C). Mutation of *DCL3* has a lesser effect on CNN methylation, again suggesting partial compensation by other Dicers. Collectively, the data of Figures 1A–1C indicate that the loss of endogenous repeat siRNAs correlates with the loss of both CG and CNN methylation, implicating RNA-directed DNA methylation (Aufsatz et al., 2002; Cao et al., 2003).

To facilitate cytological and biochemical studies, we developed transgenic lines that express functional, epitope-tagged versions of the proteins involved in the nuclear siRNA pathway. Genomic-clone transgenes expressing NRPD1a, NRPD1b, or DCL3 bearing C-terminal FLAG epitope tags all rescued their corresponding mutations and restored siRNA production, as did a YFP-RDR2 fusion engineered using a full-length *RDR2* cDNA (Figure 1D). The *NRPD1a* and *NRPD1b* transgenes also restored cytosine methylation at 5S gene repeats (Figure 1E). Collectively, these results indicate that the recombinant proteins retain their biological functions.

The Alternative Pol IV Largest Subunits, NRPD1a and NRPD1b, Physically Interact with NRPD2

Genetic evidence suggests that the Pol IV second largest subunit NRPD2 interacts with NRPD1a or NRPD1b within Pol IVa or Pol IVb, respectively (Herr et al., 2005; Kanno et al., 2005; Onodera et al., 2005; Pontier et al., 2005). To obtain biochemical evidence for such interactions, we exploited transgenic plants expressing FLAG-tagged NRPD1a or NRPD1b and an anti-NRPD2 antibody (Onodera et al., 2005) to ask whether NRPD2 associates with the alternative largest subunits in vivo. Indeed, NRPD2 coimmunoprecipitates with both NRPD1a-FLAG and NRPD1b-FLAG in multiple independent transgenic plants (Figures 1F and 1G). The quantity of

(F) Physical interaction between Pol IVa subunits NRPD1a and NRPD2 detected by coimmunoprecipitation. Proteins from multiple independent NRPD1a-FLAG transgenic lines were immunoprecipitated using anti-FLAG antibody, then subjected to SDS-PAGE and electroblotting. Membranes were sequentially analyzed to detect the FLAG epitope (top) and NRPD2 (bottom).

(G) Physical interaction between NRPD1b and NRPD2. The experiment was performed as for (F) using multiple independent NRPD1b-FLAG transgenic lines.

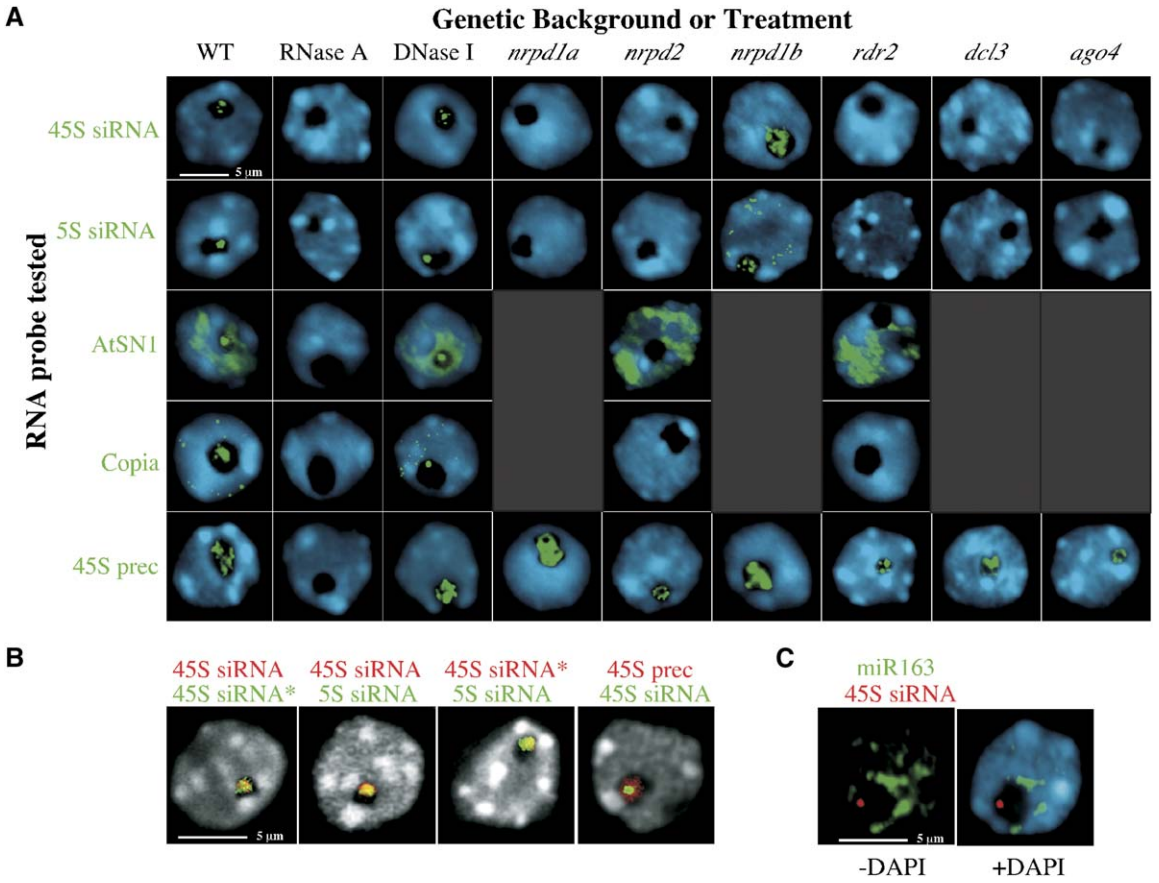

Figure 2. Nuclear Localization of siRNAs

(A) RNA-FISH using the same probe sequences used for the RNA blots of Figure 1A was performed in wild-type, nuclease-treated, or mutant nuclei as indicated. As a control, a probe that detects the 45S rRNA precursor transcripts was also used. Nuclei were counterstained with DAPI (blue). Size bars represent 5 μm in all panels.

(B) Different siRNAs colocalize within the nucleolus. Simultaneous detection of RNA target pairs was performed using two-color FISH. Three-dimensional projections of five to seven optical sections obtained by multiphoton microscopy are shown. The red or green color of the lettering corresponds to the color of the signal for the indicated probes. Nuclei were counterstained with DAPI (false colored gray in these images). Thirty-five nuclei were observed for each probe combination. In all nuclei examined, at least 50% of the green and red pixels overlapped in the digital images to yield yellow signals.

(C) Two-color FISH using the 45S siRNA probe (red) and miR163 probe (green). Nuclei were counterstained with DAPI (blue). A localization pattern like that shown was observed in all 155 nuclei examined.

coimmunoprecipitated NRPD2 is proportional to the abundance of NRPD1a or NRPD1b in the different lines, as expected of subunits with fixed stoichiometries.

siRNAs Are Concentrated within the Nucleolus

It is not known where endogenous siRNAs are generated or processed within the cell. So, to detect siRNAs or their precursors, we employed RNA fluorescence in situ hybridization (RNA-FISH) with digoxigenin- or biotin-labeled probes (Figure 2A) identical in sequence to those used for siRNA blot hybridization (see Figure 1A). With all siRNA probes, an intense hybridization signal was observed within the nucleolus, which is the region of the nucleus not stained appreciably by the fluorescent DNA binding dye DAPI. This was true of leaf mesophyll cells at interphase, as shown throughout this paper, and in root meristem cells (O.P., unpublished data). In the case of the *AtSN1* probe, a diffuse signal was also observed throughout the nucleoplasm. The nucleolar dots detected with siRNA probes occupy a small portion of the nucleolus when compared to the 45S pre-rRNA precursor transcripts that are generated by RNA polymerase I and processed in the nucleolus (Figure 2A, bottom row).

Hybridization signals detected using different siRNA probes colocalized, as shown using two-color RNA-FISH with probes specific for 45S siRNAs corresponding to opposite DNA strands (45S siRNA and 45S siRNA*) or 5S siRNAs (Figure 2B). These siRNA probe signals are spatially distinct from the signals obtained using a miRNA probe (Figure 2C). Collectively, these data indicate that nuclear siRNA hybridization signals localize within a discrete compartment of the nucleolus, smaller than the

volume occupied by 45S pre-rRNA and distinct from sites where miRNA or their precursors are concentrated.

As shown in Figure 2A, siRNA and pre-rRNA hybridization signals are eliminated if nuclei are treated with ribonuclease A (RNase A) prior to extensive washing and probe hybridization but are not affected by DNase I treatment. These tests suggest that the hybridization signals result from the RNA probes' annealing to RNA targets. Importantly, the nucleolar dot signals are absent in *nrpd2*, *nrpd1a*, *rdr2*, *dcl3*, or *ago4* mutants, and, typically, no signal is observed elsewhere (although low-intensity, dispersed signals occurred infrequently; see Table S1 in the Supplemental Data available with this article online for quantitative data). The exception is *nrpd1b*, for which dispersal of the nucleolar dot (as shown in Figure 2A) is more common than complete loss of signal (see Table S1). In general, these observations are consistent with the RNA blot hybridization data (Figure 1A). Importantly, 45S pre-rRNAs are unaffected by the siRNA pathway mutations, as expected.

The loss of hybridization signals in the mutants, including *dcl3* and *ago4*, which should act downstream of siRNA precursor formation, suggests that we are detecting siRNAs in the nucleolar dots rather than precursors. Perhaps the latter escape detection because they are dispersed throughout the nucleus and not concentrated in one location. However, the *AtSN1* signals, external to the nucleolus, that persist in the mutants might be precursor RNAs.

Nucleolar siRNA Processing Centers

The detection of nuclear siRNAs prompted us to ask where the proteins of the nuclear siRNA pathway are located. NRPD1a, NRPD1b, RDR2, DCL3, and AGO4 were immunolocalized in transgenic nuclei by virtue of their epitope or YFP tags, whereas native NRPD2 was localized using an anti-peptide antibody (Figure 3A, top row). NRPD1a and NRPD2, the known subunits of Pol IVa, showed similar, punctate localization patterns; significantly, neither protein associates with the nucleolus. By contrast, FLAG-tagged NRPD1b, the largest subunit of Pol IVb, localizes within a nucleolar dot in addition to puncta external to the nucleolus (see also Li et al., 2006 [this issue of *Cell*] and Table S2). RDR2, DCL3, and AGO4 also display prominent nucleolar dot signals in addition to puncta or diffuse signals outside the nucleolus. RDR2 signals are distinctive in that a ring or crescent at the perimeter of the nucleolus is typically observed in addition to the nucleolar dot, and this is true for both epitope-tagged and native RDR2. Control experiments showed that no immunolocalization signals were detected in transgenic nuclei if primary antibodies were omitted; likewise, no signals were detected in wild-type nuclei using anti-FLAG, anti-Myc, or anti-YFP antibodies (see Figure S1).

Nucleolar dot signals can be observed at the center or the periphery of the nucleolus, consistent with data of Li et al. (2006) showing that AGO4 colocalizes with markers of nucleolar accessory bodies, or Cajal bodies (Cioce and Lamond, 2005). Cajal bodies are dynamic nuclear organelles that can move in and out of nucleoli (Boudonck et al., 1999) and are implicated in the assembly of RNA-protein complexes, including snRNPs and snoRNPs (Cioce and Lamond, 2005). Therefore, what we call nucleolar dots throughout this paper are likely to be Cajal bodies or related entities (see Li et al., 2006).

Treating nuclei with RNase A prior to antibody incubation caused a complete loss of signal for all of the proteins in the majority of nuclei examined, suggesting that the proteins are not retained in RNA-depleted nuclei (Figure 3A). However, a minority of the nuclei continued to show wild-type protein localization patterns, albeit at reduced intensity, suggesting that not all nuclei are equally accessible to RNase treatment (see Table S2). Further analysis showed that, whereas NRPD2, NRPD1a, and NRPD1b signals are lost from RNase A-treated nuclei, the proteins are not lost from DNase I-treated nuclei, although NRPD1b and NRPD2 are partially mislocalized (Figure 3B and Figure S2, green signals). Conversely, the signals for the second largest subunit of DNA-dependent RNA polymerase II are lost upon DNase, but not RNase, treatment (Figure 3B, red signals). Collectively, these observations suggest that Pol IV interacts with RNA rather than DNA templates, unlike Pol II.

Using anti-epitope antibodies that detect transgene-encoded recombinant proteins, in combination with anti-peptide antibodies recognizing the native proteins, we simultaneously localized pairs of proteins using two-color immunofluorescence (Figure 3C; Table S3). The native proteins and the recombinant proteins were found to display the same localization patterns, indicating that the anti-peptide antibodies are specific for their targets and that the epitope tags do not disrupt recombinant protein localization. NRPD1a and NRPD2, the subunits of Pol IVa, colocalize precisely, resulting in yellow signals (Figure 3C, top row; note that differences in intensity of the green and red signals influence the apparent extent of overlap). Slightly more than half of the NRPD1b foci external to the nucleolus colocalize with the NRPD1a/NRPD2 foci (Figure 3C, second row from top), suggesting that Pol IVb occurs at approximately half of the Pol IVa foci. However, the remaining NRPD1b foci are spatially distinct from NRPD2 (and NRPD1a). A conclusion from the latter observation is that the Pol IVb largest subunit can exist apart from the second largest subunit, both external to the nucleolus and within the nucleolus, where no NRPD2 is detectable.

External to the nucleolus, NRPD1a, NRPD2, and NRPD1b do not colocalize with RDR2, DCL3, or AGO4. However, the portion of the NRPD1b pool that is nucleolus associated colocalizes with RDR2, DCL3, and AGO4 within the nucleolar dot (Figure 3C).

We next asked whether the nucleolar dots previously detected by RNA-FISH (Figure 2) correspond to the same nucleolar dots where NRPD1b, RDR2, DCL3, and AGO4 colocalize (Figure 3). To address this question, we performed protein immunolocalization followed by

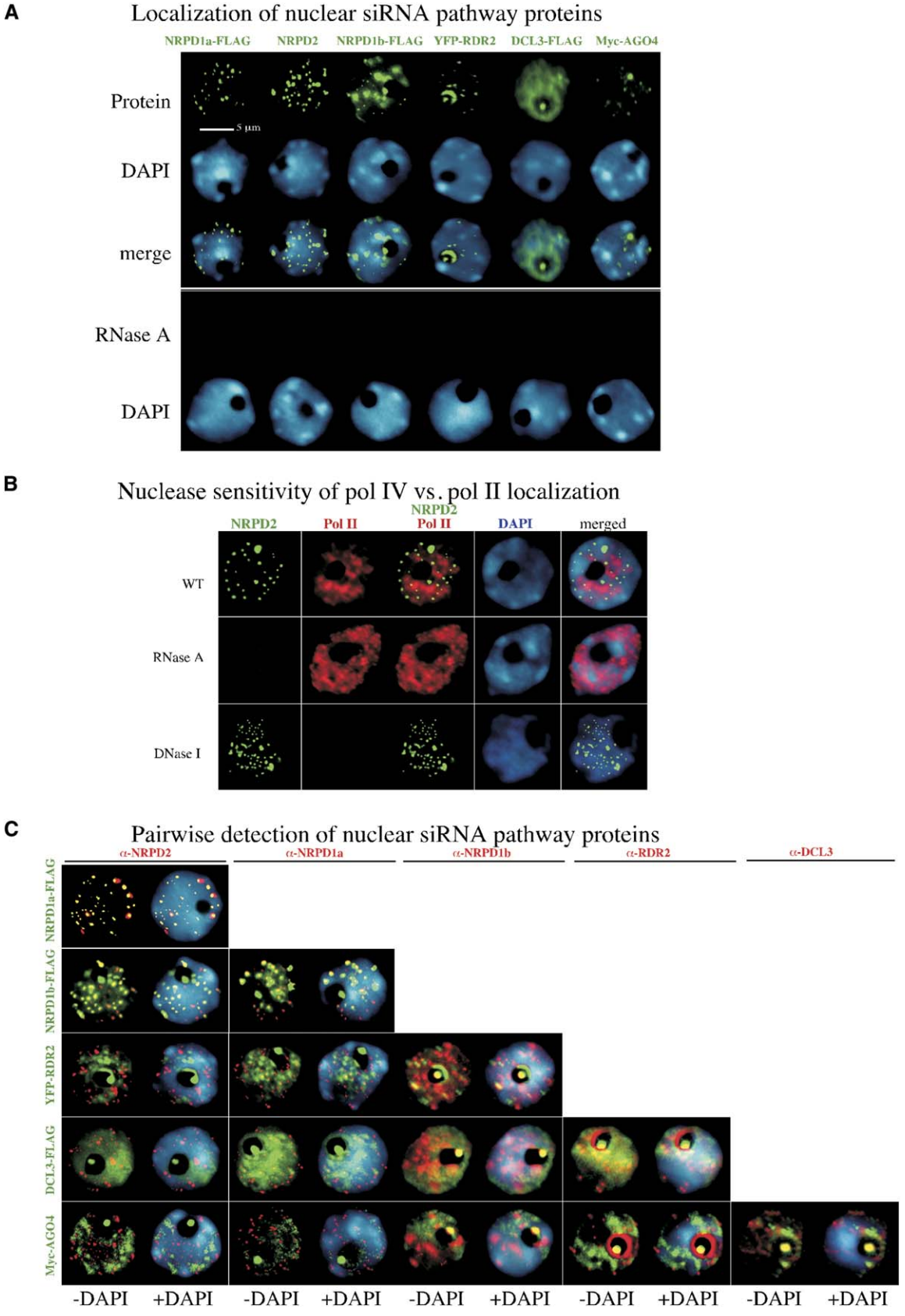
A
Localization of nuclear siRNA pathway proteins
NRPD1a-FLAG
NRPD2
NRPD1b-FLAG
YFP-RDR2
DCL3-FLAG
Myc-AGO4
Protein
5 μm
DAPI
merge
RNase A
DAPI
B
Nuclease sensitivity of pol IV vs. pol II localization
NRPD2
Pol II
NRPD2
Pol II
DAPI
merged
WT
RNase A
DNase I
C
Pairwise detection of nuclear siRNA pathway proteins
α-NRPD2
α-NRPD1a
α-NRPD1b
α-RDR2
α-DCL3
NRPD1a-FLAG
NRPD1b-FLAG
YFP-RDR2
DCL3-FLAG
Myc-AGO4
-DAPI
+DAPI
-DAPI
+DAPI
-DAPI
+DAPI
-DAPI
+DAPI
-DAPI
+DAPI

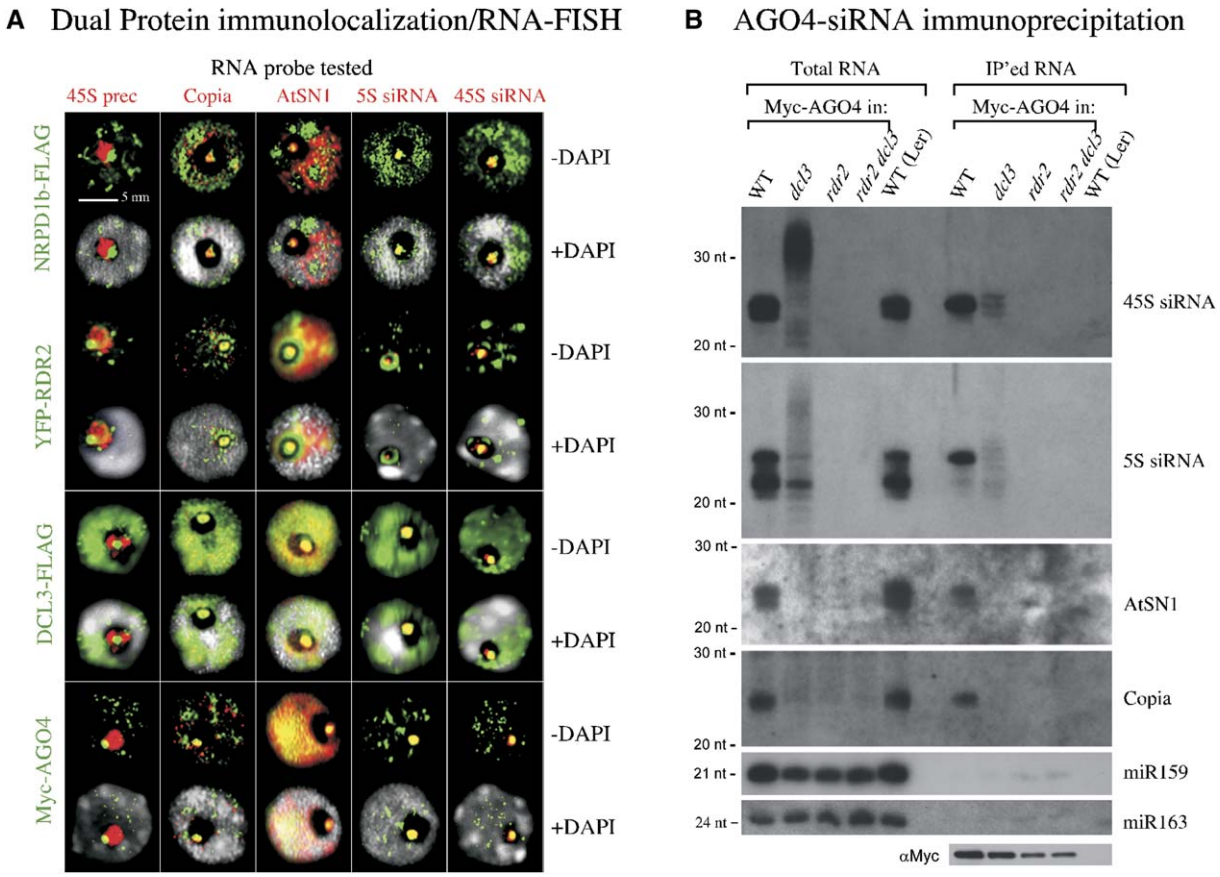

Figure 4. siRNAs Colocalize with NRPD1b, RDR2, DCL3, and AGO4

(A) Nuclei were hybridized with 45S rRNA precursor, *Copia*, *AtSN1*, 5S siRNA, or 45S siRNA probes (red signals). NRPD1b-FLAG, YFP-RDR2, DCL3-FLAG, or Myc-AGO4 was immunolocalized using anti-FLAG, anti-YFP, or anti-Myc antibodies (green signals). Images shown are three-dimensional projections of five to seven optical sections obtained by multiphoton microscopy. Pairs of images are presented for each protein localized, the lowermost image including the DAPI signal (false colored gray) to help reveal the nucleolus.

(B) siRNAs physically associate with AGO4. Total RNA or RNA immunoprecipitated (IP) using anti-Myc antibodies from transgenic plants expressing Myc-AGO4 in wild-type, *dcl3*, *rdr2*, or *dcl3 rdr2* backgrounds was subjected to RNA blot hybridization using 45S siRNA, 5S siRNA, *AtSN1*, *Copia*, and miR159 probes. RNA of nontransgenic wild-type plants (ecotype Ler) served as a control. The presence of AGO4 in immunoprecipitates was confirmed by immunoblotting using anti-Myc antibody.

RNA-FISH (Figure 4A). As is evident by the yellow signals resulting from siRNA probe and protein signal overlap, NRPD1b, RDR2, DCL3, and AGO4 typically colocalize with 45S, 5S, *AtSN1*, and *Copia* siRNAs within the nucleolar dots but do not colocalize precisely with 45S rRNA precursor transcripts (Figure 4A; see also Table S4). We interpret the colocalization of NRPD1b, RDR2, DCL3, AGO4, and siRNAs as evidence of siRNA processing centers in which dsRNAs generated by RDR2 are diced by DCL3 to generate siRNAs that are loaded into RISC effector complexes that contain AGO4 and NRPD1b.

Consistent with the interpretation that siRNAs are stably associated with AGO4, immunoprecipitation of Myc-AGO4 pulls down 45S, 5S, *AtSN1*, and *Copia* siRNAs (Figure 4B). Moreover, in *rdr2* or *rdr2 dcl3* double mutants, siRNAs are no longer found in the Myc-AGO4 immunoprecipitates. In *dcl3* mutants, siRNAs associated with AGO4 are greatly reduced in abundance and variable in size, consistent with the hypothesis that AGO4 is capable of binding siRNAs generated by other Dicers that partially compensate for the loss of DCL3.

Figure 3. Immunolocalization of Nuclear siRNA Pathway Proteins

(A) Epitope-tagged NRPD1a, NRPD1b, DCL3, and AGO4 recombinant proteins that rescue corresponding mutations were immunolocalized (green signals) using anti-FLAG or anti-Myc antibodies. Native NRPD2 was detected using anti-peptide antisera. RDR2-YFP was localized using anti-YFP. Nuclei were counterstained with DAPI.

(B) Immunolocalization of NRPD2 and the Pol II second largest subunit in wild-type untreated, RNase A-, or DNase I-treated nuclei.

(C) Anti-peptide antibodies recognizing native proteins (red signals) were used in combination with antibodies recognizing FLAG-, Myc-, or YFP-tagged recombinant proteins (green signals) in nuclei of transgenic plants. Colocalizing proteins generate yellow signals.

Pol IV and the Putative Chromatin Remodeler DRD1 Colocalize with Endogenous Repeats

To determine where the endogenous DNA repeats are located relative to the nucleolar dots, we used DNA-FISH to localize the 45S rRNA gene loci (i.e., the nucleolus organizer regions; NORs) and 5S rRNA gene clusters. The FISH signals for the highly condensed portions of 45S and 5S rRNA gene loci are not detected within the nucleolus (Figure 5, red signals), indicating that the bulk of the target gene loci, composed mostly of inactive repeats, are distant from the nucleolar dots.

By combining protein immunolocalization (green signals) with DNA-FISH (red signals), we asked whether the Pol IV foci external to the nucleolus correspond to endogenous repeat loci. Indeed, NORs and 5S gene loci were found to colocalize with NRPD1a, NRPD1b, and NRPD2, yielding yellow signals at most, though not all, of the loci (see Table S5 for quantitative data). Some overlap between 5S gene loci and RDR2 or DCL3 signals was also observed, although the diffuse distribution of DCL3 may make the apparent overlap coincidental. We also examined the localization of DRD1, a SWI2/SNF2-related protein that is involved in RNA-directed DNA methylation via a Pol IVb-dependent pathway (Kanno et al., 2005; Kanno et al., 2004). DRD1 is distributed throughout the nucleus, with the exception of the nucleolus, and is concentrated at chromocenters that include NORs and 5S gene loci (Figure 5, bottom row). Collectively, these observations suggest that Pol IVa, Pol IVb, and DRD1 are present at the endogenous repeat loci, presumably acting in the generation of siRNA precursors or in the downstream functioning of siRNA-containing effector complexes.

Mutation-Induced Mislocalization of Nuclear siRNA Pathway Proteins

To deduce the order in which proteins of the nuclear siRNA pathway act, we examined the effect of mutations on each protein's localization, resulting in the matrix of images shown in Figure 6 (see Table S6 for quantitative data). Protein signals were absent upon mutation of the genes that encode the corresponding proteins, as expected, indicating that all of the mutants are protein nulls and that the antibodies are specific for their intended targets. NRPD1a localization is unaffected in *rdr2*, *dcl3*, or *ago4* mutants, as is NRPD2 localization, consistent with Pol IVa acting upstream of RDR2, DCL3, and AGO4. RDR2 localization is dependent on Pol IVa (NRPD1a and NRPD2), but not on NRPD1b, DCL3, or AGO4, indicating that RDR2 acts downstream of Pol IVa, but upstream of Pol IVb, dicing and effector complex assembly.

DCL3 localization is dependent on both Pol IVa and RDR2 but is independent of AGO4 and NRPD1b, suggesting that dicing occurs following double-stranded RNA formation, mediated by RDR2, and upstream of effector complex assembly and Pol IVb function. Consistent with this interpretation, the NRPD1b nucleolar dot is absent in *nrpd1a*, *rdr2*, *dcl3*, and *ago4* mutants but is still present in a *drd1* mutant (see Figure S3), indicating that the nucleolar NRPD1b signal is dependent on siRNA processing and effector complex assembly but is formed upstream of steps that involve chromatin remodeling by DRD1. The NRPD1b signals that are outside the nucleolus are unaffected in *rdr2* or *dcl3* mutants but are less punctate and therefore appear more diffuse in the *drd1* mutant, suggesting that DRD1 influences NRPD1b localization at target loci.

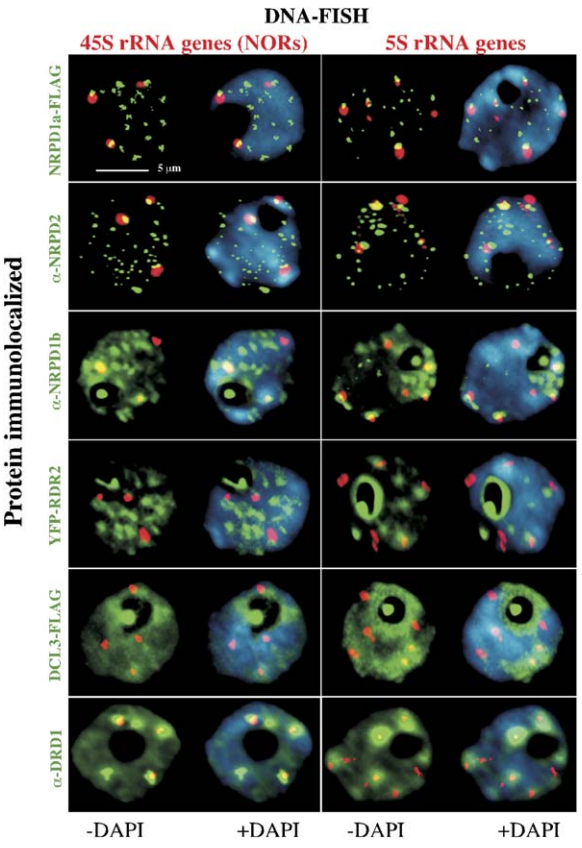

Figure 5. Pol IV Colocalizes with Endogenous Repeat Loci

45S rRNA gene loci (nucleolus organizer regions; NORs) or 5S gene chromosomal loci were visualized using DNA-FISH (red signals), and the indicated proteins were immunolocalized (green signals). Yellow indicates overlapping DNA and protein signals. NRPD1a-FLAG and DCL3-FLAG recombinant proteins were detected in nuclei of transgenic plants using anti-FLAG antibodies; NRPD2, NRPD1b, and DRD1 were detected in nuclei of nontransgenic plants using anti-peptide antibodies recognizing the native proteins; and recombinant YFP-RDR2 was detected using anti-YFP (green signals). Nuclei were counterstained with DAPI (blue). Note that *A. thaliana* has four NORs and six 5S gene loci in the Col-0 ecotype. The NORs tend to coalesce such that only three NORs are observed in most of the images shown.

DISCUSSION

A Spatial and Temporal Model for the Nuclear siRNA Pathway

RNA-directed DNA methylation requires de novo methyltransferase activity, suggesting that DRM-class cytosine

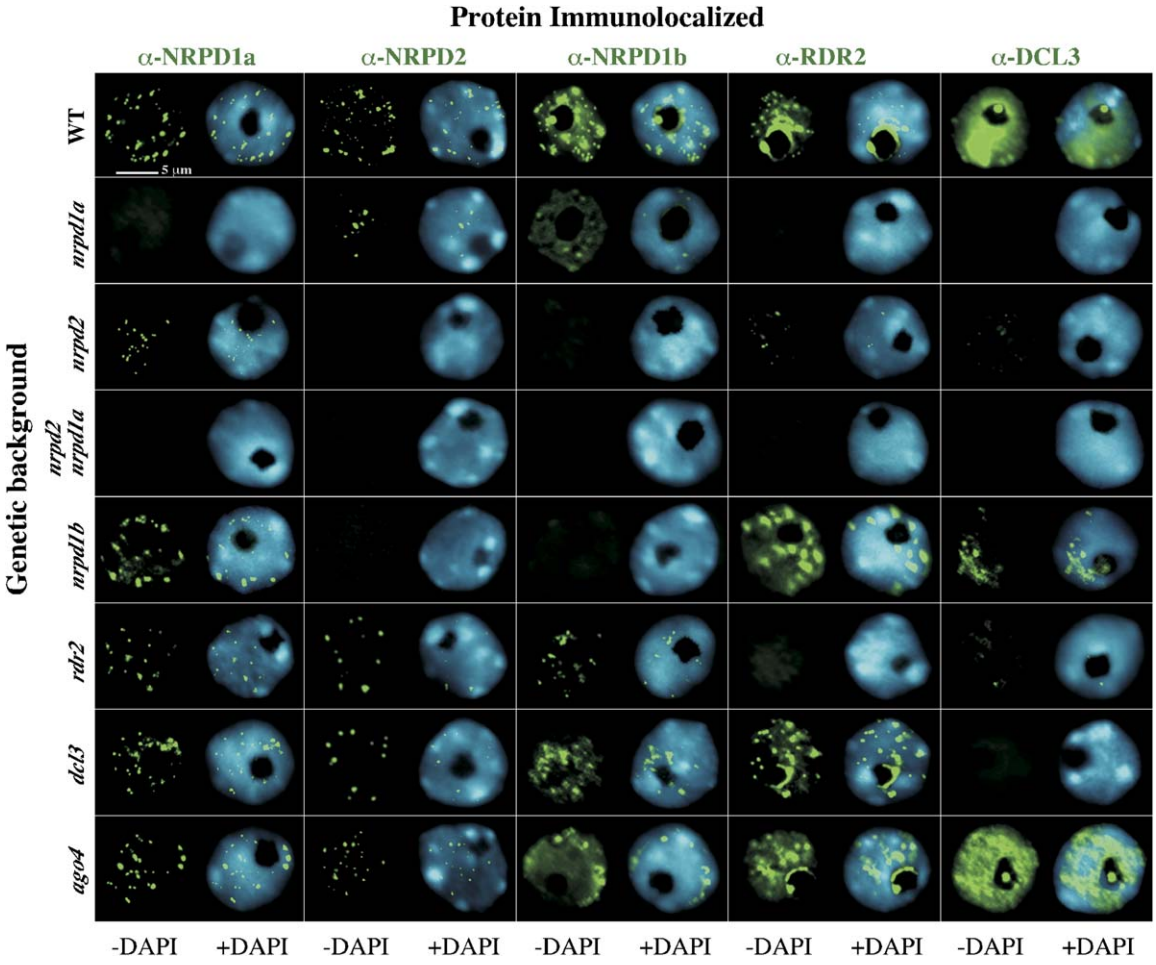

Figure 6. Effects of Mutations on the Localization of Proteins Involved in Nuclear siRNA Biogenesis

The figure shows a matrix of images in which NRPD1a, NRPD2, NRPD1b, RDR2, and DCL3 were immunolocalized using anti-peptide antibodies recognizing the native proteins (green signals) in multiple genetic backgrounds as indicated along the vertical axis. Nuclei were counterstained with DAPI (blue).

methyltransferases (probably *DRM2* only, because *DRM1* is not expressed appreciably) act downstream of siRNA production (Cao et al., 2003). However, endogenous nuclear siRNAs fail to accumulate in *drm* mutants (Xie et al., 2004; Zilberman et al., 2004), suggesting that DRM2 also acts upstream of siRNA production (see also Figure 1A). Our model attempts to address this apparent paradox (Figure 7). Based on a study in *Neurospora* suggesting that methylation impedes RNA polymerase elongation (Rountree and Selker, 1997), we propose that transcripts trailing from polymerases that are stalled or slowed by DRM-mediated methylation (Figure 7, upper left) are sensed as aberrant and, directly or indirectly, become templates for Pol IVa. In this model, Pol IVa is spatially tethered to the DNA by virtue of the RNA template. This aspect of the model accounts for the colocalization of Pol IVa subunits with endogenous repeat loci and their loss in RNase A-treated nuclei. We place Pol IVa first in the pathway because Pol IVa is located directly at the endogenous repeat loci and because mutation of either Pol IVa subunit (NRPD1a or NRPD2) eliminates siRNA production. By contrast, mutation of NRPD1b, the largest subunit of Pol IVb, which also colocalizes with the endogenous repeat loci, does not eliminate siRNA production but does affect RNA-directed cytosine methylation, suggesting that Pol IVb acts late in the pathway (Kanno et al., 2005; Pontier et al., 2005; Vaucheret, 2005; see also Figures 1A–1C). The fact that siRNA accumulation is reduced in *nrpd1b* mutants (see Figure 1A) may be due to the destabilization of the NRPD2 pool upon loss of NRPD1b (see Figure 1G, Figure 6 and Pontier et al., 2005). Loss of NRPD2 would indirectly deplete Pol IVa activity by depriving NRPD1a of its partner catalytic subunit. Alternatively, decreased Pol IVb-dependent cytosine methylation might decrease the incidence of aberrant transcript production at endogenous repeat loci, thereby depleting the pool of Pol IVa templates. These alternative explanations are not mutually exclusive.

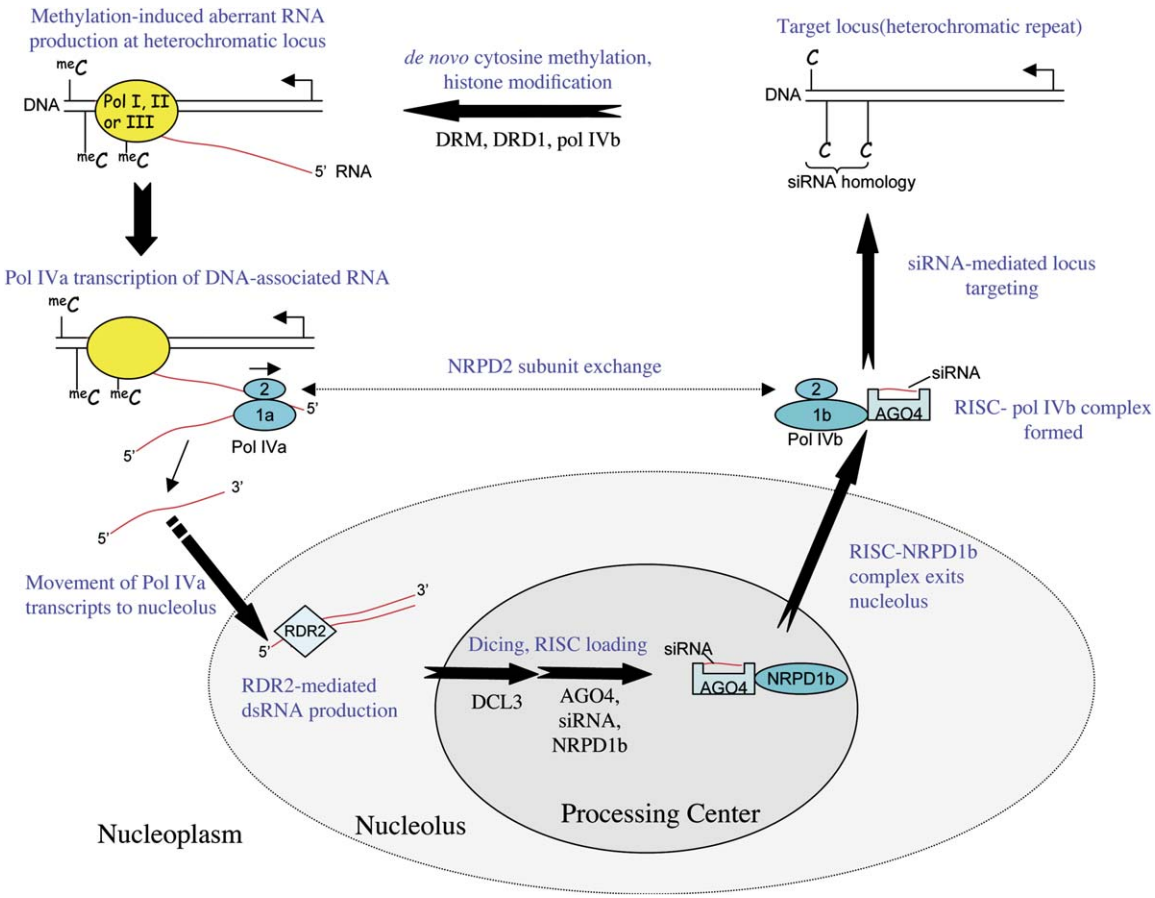

Figure 7. A Spatial and Temporal Model for Nuclear siRNA Biogenesis

Subunits of Pol IVa (abbreviated 1a and 2) colocalize with endogenous repeat loci but are mislocalized upon RNase A treatment, suggesting that Pol IVa transcribes RNA templates whose spatial distribution is influenced by DNA. We propose that cytosine methylation by DRM induces the production of aberrant RNAs, possibly by impeding polymerase elongation, which Pol IVa then uses as templates. Pol IVa transcripts then move, by an unknown mechanism, to the nucleolus, where RDR2, DCL3, and AGO4 are located. In the siRNA processing center, the largest subunit of Pol IVb, NRPD1b, joins the AGO4-containing RISC complex and acquires the NRPD2 subunit to become functional Pol IVb only upon leaving the nucleolus. Formation of Pol IVb is required for the stability of the NRPD2 pool despite the fact that NRPD2 colocalizes more precisely with NRPD1a than with NRPD1b, suggesting that NRPD2 subunits exchange between Pol IVa and b. AGO4, Pol IVb, and DRD1 then play unspecified roles in guiding heterochromatic modifications at the endogenous repeats, including de novo cytosine methylation by DRM. Methylation-dependent production of aberrant RNAs results in a positive feedback loop for maintaining heterochromatin at the DNA repeats.

Like Pol IVa, RDR2 is required for endogenous siRNA production. RDR2 is mislocalized in an *nrpd1a* mutant, whereas the converse is not true (see Figure 6), indicating that RDR2 acts downstream of Pol IVa. RDR2 is not abundant at the endogenous repeats but is concentrated in the nucleolus. Collectively, these observations suggest that Pol IVa generates precursor RNAs at the endogenous repeats and that these transcripts then move to the nucleolus, where their complements are generated by RDR2 transcription. Annealing of these RNAs would produce dsRNAs that are then diced by DCL3 and loaded into an AGO4-containing effector complex, or RISC (RNA-induced silencing complex), within the siRNA processing center. The observation that Pol IVa subunits and RDR2 are not mislocalized in *dcl3* or *ago4* mutants is consistent with Pol IVa and RDR2 acting upstream of DCL3 and AGO4. Likewise, the absence of siRNAs associated with AGO4 in *rdr2* mutants, the atypical sizes of siRNAs associated with AGO4 in *dcl3* mutants, and the mislocalization of AGO4 in *rdr2* or *dcl3* mutants (see also Li et al., 2006) indicate that AGO4 acts downstream of RDR2 and DCL3.

Two observations suggest that Pol IVb acts downstream of AGO4-RISC assembly. First, the largest subunit of Pol IVb, NRPD1b, colocalizes with the nucleolar dot, but only if siRNAs are being produced and assembled into effector complexes; the nucleolar NRPD1b signal is absent in *nrpd1a*, *rdr2*, *dcl3*, or *ago4* mutants. Second, the NRPD2 subunit is never observed within the nucleolus yet is presumably essential for Pol IVb function based on the genetic screen of Kanno et al. that recovered nine mutant alleles of *NRPD1b* and 12 alleles of *NRPD2a* but no alleles of *NRPD1a* (Kanno et al., 2005). The genetic evidence

strongly predicts that NRPD1b is nonfunctional in the absence of the second largest subunit. We propose that NRPD1b associates with AGO4-RISC, which is supported by our immunolocalization data and the finding that NRPD1b can be coimmunoprecipitated in association with AGO4 (Li et al., 2006). Upon leaving the nucleolus as a subunit of AGO4-RISC, we deduce that NRPD1b can then associate with NRPD2, forming functional Pol IVb. Consistent with this hypothesis, NRPD2 coimmunoprecipitates with AGO4 (J.H. and C.S.P., unpublished data) as well as with NRPD1b (see Figure 1G).

How AGO4-RISC-Pol IVb complexes mediate their effects on chromatin modification at target loci is unclear. One possibility is that AGO4-RISC directs Pol IVb to its target sites. Alternatively, AGO4 might transfer the siRNA to Pol IVb when the NRPD2 subunit joins the NRPD1b subunit, after the AGO4-RISC-NRPD1b complex leaves the nucleolus. The siRNA, or a Pol IVb transcript primed by the siRNA, might then be used to conduct a homology search for target sequences, aided by DRD1 (Kanno et al., 2004), a member of the SWI2/SNF2-related family of chromatin-remodeling ATPases that is within a subfamily most closely related to yeast RAD54. In double-strand DNA break repair, RAD54 is required for helping broken DNA ends conduct a homology search and invade homologous duplex DNA of a sister chromosome, thereby facilitating repair by homologous recombination (Krogh and Symington, 2004). A partnership between Pol IVb and DRD1 could account for their presence at the target loci, the observation that NRPD1b and DRD1 are both essential for cytosine methylation but not siRNA production (Kanno et al., 2004, 2005), and the partial mislocalization of NRPD1b in a *drd1-6* mutant (see Figure S2). Moreover, RNA polymerases and chromatin-remodeling ATPases are nucleotide triphosphate-hydrolyzing molecular motors that can be envisioned working together, with processive movement of the polymerase possibly providing directionality to subsequent chromatin modifications. Resulting de novo DNA methylation by DRM2, which is predicted to contribute to aberrant RNA production, would provide for positive feedback in our model (Figure 7).

As touched upon previously, our observation that NRPD2 signals are severely reduced in *nrpd1b*, more so than in the *nrpd1a* mutant (see Figure 1G and Figure 6), is consistent with previously published immunoblot data (Pontier et al., 2005). Nonetheless, it is surprising given the nearly perfect colocalization of NRPD2 with NRPD1a, as opposed to only ~50% overlap of NRPD2 with NRPD1b (see Figure 3C). Based on these data, one might expect NRPD1a to be most important for NRPD2 stability. To reconcile these findings, we propose that NRPD2 must be able to exchange between Pol IVb and Pol IVa (Figure 7), with NRPD1b interactions somehow more important for the overall stability of the NRPD2 pool.

The idea that incomplete, or otherwise aberrant, transcripts can induce transcriptional silencing at endogenous repeats may have parallels with the silencing of nonproductive human immunoglobulin genes. In this phenomenon, genes whose transcripts contain premature stop codons following V-D-J recombination are transcriptionally silenced (Buhler et al., 2005), indicating a link between nonsense-mediated decay (NMD) and chromatin modification. In *Arabidopsis*, proteins of the exon-joining complex and NMD pathways were identified within the nucleolar proteome, and some were shown to localize as nucleolar dots (Pendle et al., 2005). Whether these proteins colocalize with the siRNA processing centers is unclear at present.

The nucleolus is best known as the site of 45S pre-rRNA transcription and ribosome assembly. However, small-RNA-directed pre-rRNA cleavage, methylation, and pseudouridylation; biogenesis of signal-recognition particle and telomerase small RNAs; tRNA processing by RNase P; and some pre-mRNA processing also take place within the nucleolus (Bertrand et al., 1998; Filipowicz and Pogacic, 2002; Kiss, 2002; Pederson, 1998). Our findings suggest that processing of endogenous nuclear siRNAs, and possibly RISC storage or sequestration, are additional nucleolar functions to be explored.

EXPERIMENTAL PROCEDURES

Mutant Plant Strains

Arabidopsis rdr2-1 and *dcl3-1* were provided by Jim Carrington, *sgs2-1* (alias *sde1*; *rdr6*) was provided by Herve Vaucheret, and *drd1-6* was provided by Tatsuo Kanno and Marjori Matzke. *drm2-1*, *ago4-1*, and *nrpd1b-11* (SALK_029919) were obtained from the Arabidopsis Biological Resource Center. *nrpd1a* and *nrpd2* mutants were described previously (Onodera et al., 2005).

Generation of Transgenic Lines

Full-length genomic sequences including promoters were amplified by PCR from *A. thaliana* Col-0 DNA using Pfu polymerase (Stratagene) and cloned into pENTR/D-TOPO (Invitrogen). NRPD1a primers were 5′-CACCGGTGTCTCACATTCCAAAGTCCCC-3′ (forward) and 5′-CGGGTTTTCGGAGAAACCACC-3′ (reverse). *NRPD1b* primers were 5′-CACCGCGTACTACAAACGGAAACGGTCA-3′ and 5′-TGTCTGCG TCTGGGACGG-3′. Genomic DCL3 was amplified from BAC clone T15B3 using 5′-CACCCCGACCGAAATCCTCATGACCTAA-3′ and 5′-CTTTTGTATTATGACGATCTTGCGGCGC-3′; the CACC added to forward primers allowed directional cloning into the entry vector. Reverse primers eliminated stop codons to allow epitope-tag fusion. Genes were recombined into pEarleyGate 302 (Earley et al., 2006) to add C-terminal FLAG epitopes. RDR2 coding sequences were amplified by RT-PCR using Pfx Platinum DNA polymerase (Invitrogen) and primers 5′-CACCATGGTGTCAGAGACGACGAC-3′ and 5′-GGGCAATCAAAT GGATACAAGTCC-3′. PCR products captured in pENTR/D-TOPO were recombined into pEarleyGate 104 (Earley et al., 2006), fusing RDR2 sequences C-terminal to YFP expressed from a CaMV 35S promoter. Transformation of constructs into corresponding homozygous mutants was by the floral dip method (Clough and Bent, 1998).

Southern Blotting and Small-RNA Blot Hybridization

Genomic DNA (250 ng) digested with HaeIII or HpaII was subjected to agarose gel electrophoresis, blotted to nylon membranes, and hybridized to a 5S gene probe as described previously (Onodera et al., 2005). Generation of RNA probes labeled with [α-^{32}P]CTP and small-RNA blot hybridization were also as described previously (Onodera et al., 2005). Specific oligodeoxynucleotides used in T7 polymerase reactions (CCTGTCTC hybridized to the T7 promoter adaptor) were as follows: 45S siRNA: 5′-CAATGTCTGTTGGTGCCAAGAGGGAAAAG

GGCCCTGTCTC-3′; 45S prec: 5′-AGTCCGTGGGGAACCCCCTTTT TCGGTTCGCCCCTGTCTC-3′; 5S siRNA: 5′-AGACCGTGAGGCCAA ACTTGGCATCCTGTCTC-3′; *Copia*: 5′-TTATTGGAACCCGGTTAGG ACCTGTCTC-3′, and miR163: 5′-TTGAAGAGGACTTGGAACTTCG ATCCTGTCTC-3′.

Antibodies

Rabbit antibodies raised against NRPD2 and Pol II second-largest-subunit peptides were described previously (Onodera et al., 2005). Chicken antibodies recognizing DCL3, NRPD1a, NRPD1b, or RDR2 were generated against peptides conjugated to keyhole limpet hemocyanin. Peptides were as follows: DCL3: SLEPEKMEEGGGSNC; NRPD1a: EELQVPVGTLTSIGC; NRPD1b: MEEESTSEILDGEIC; RDR2: ETTTNRSTVKISNVC; DRD1: NKNVHKRKQNQVDDGC. Immunolocalization was performed using 1:200 dilutions of antisera, except that NRPD1b antiserum was diluted 1:500. FLAG-tagged proteins were detected using mouse monoclonal anti-FLAG antibody (Sigma-Aldrich) diluted 1:400. RDR2-YFP was detected using mouse anti-GFP/YFP (BD Biosciences) diluted 1:500.

Immunolocalization

Leaves from 28-day-old plants were harvested and nuclei were extracted as described previously (Onodera et al., 2005). After postfixation in 4% paraformaldehyde/PBS (phosphate-buffered saline), washes in PBS, and blocking at 37°C, slides were exposed overnight to primary antisera in PBS and 0.5% blocking reagent (Roche). After washes in PBS, slides were incubated at 37°C with anti-mouse-FITC diluted 1:100 (Sigma), goat anti-chicken Alexa 488 diluted 1:300 (Molecular Probes), or goat anti-chicken Alexa 543 diluted 1:400 (Molecular Probes). Nuclei were counterstained with 1 μg/ml DAPI (Sigma) in Vectashield (Vector Laboratories).

Immunoprecipitation and Immunoblotting of Epitope-Tagged Proteins

Pol IV immunoprecipitation was performed using protein extracted from 2.0 g of tissue according to Baumberger and Baulcombe (2005), except that homogenates were filtered through two layers of Miracloth and subjected to centrifugation at 16,000 × g for 15 min at 4°C prior to incubation with anti-FLAG M2 affinity gel (Sigma). Proteins eluted in 2× SDS-PAGE loading buffer at 100°C for 2 min were fractionated on 7.5% Tris-glycine SDS-polyacrylamide gels (Cambrex) and electroblotted to PVDF membranes (Millipore). Membranes incubated with peroxidase-linked anti-FLAG M2 antibody diluted 1:2000 (Sigma) were visualized using chemiluminescence detection (Amersham). Membranes were then stripped using 25 mM glycine-HCl (pH 2.0), 1% (w/v) SDS for 30 min with agitation, followed by two 10 min washes in Tris-buffered saline, 0.05% (v/v) Tween 20. NRPD2 immunoblotting was as described in Onodera et al. (2005).

For coimmunoprecipitation of AGO4 and siRNAs, flowers (0.7 g) frozen in liquid nitrogen were homogenized in 2 ml of IP buffer (50 mM Tris-Cl [pH 7.5], 150 mM NaCl, 5 mM $MgCl_2$, 10% glycerol, 0.1% NP-40) containing fresh DTT (2 mM), PMSF (1 mM), pepstatin (0.7 μg/ml), MG132 (10 μg/ml), and Complete protease inhibitor cocktail (Roche). Following centrifugation, lysates precleared with Protein G-agarose beads (Pierce) for 1 hr at 4°C were incubated with anti-Myc (Upstate) diluted 1:250 for 3 hr at 4°C. Antibody-antigen complexes were captured on Protein G-agarose (60 μl) at 4°C for 2 hr and washed four times with IP buffer. For siRNA detection, beads were treated with Proteinase K and extracted sequentially with TE containing 1.5%, 0.5%, or 0.1% SDS. Pooled supernatants extracted with phenol: chloroform (1:1) followed by chloroform were ethanol precipitated. Total siRNAs and RNA blots were prepared and hybridized as previously described (Mette et al., 2000; Zilberman et al., 2003). DNA probes were used to detect 5S siRNAs, 45S siRNAs, miR157, and miR163; RNA probes were used to detect *AtSN1* and *Copia* siRNAs. Probe sequences were as follows: 5S siRNA: 5′-ATGCCAAGTTTGGCCTC ACGGTCT-3′; 45S siRNA: 5′-GTCTGTTGGTGCCAAGAGGGAAAAG GGCTAAT-3′; *AtSN1*: 5′-ACCAACGTGTTGTTGGCCCAGTGGTAAA TCTCTCAGATAGAGG-3′; *Copia*: 5′-TTATTGGAACCCGGTTAGGA-3′; miR159: 5′-TAGAGCTCCCTTCAATCCAAA-3′; miR163: 5′-ATCGA AGTTGGAAGTCCTCTTCAA-3′.

RNA and DNA In Situ Hybridization

RNA probes were labeled by in vitro T7 polymerase (Ambion) transcription with digoxigenin-11-UTP or biotin-16-UTP RNA labeling mix (Roche). RNA in situ hybridization was carried out at 42°C overnight using a probe solution containing 1 μg RNA probe, 5 μg yeast tRNA (Roche), 50% dextran sulfate, 100 mM PIPES [pH 8.0], 10 mM EDTA, and 3 M NaCl as described previously (Highett et al., 1993). Slides were washed sequentially in 2× SSC, 50% formamide, 50°C followed by 1× SSC, 50% formamide, 50°C, then 1× SSC 20°C, and finally TBS at 20°C. Where applicable, nuclei were incubated at 37°C for 30 min in a solution of RNase-free DNase I (0.015 U/μl) or in a solution of RNase A (100 μg/ml, Roche). Nuclease reactions were stopped in 10 mM EDTA (pH 7.5) for 2 min followed by three washes in 0.1× SSC.

DNA-FISH using 5S or 45S rRNA gene probes labeled with biotin-dUTP or digoxigenin-dUTP was performed as described (Pontes et al., 2003). Digoxigenin-labeled probes were detected using mouse anti-digoxigenin antibody (1:250, Roche) followed by rabbit anti-mouse antibody conjugated to Alexa 488 (Molecular Probes). Biotin-labeled probes were detected using goat anti-biotin conjugated with avidin (1:200, Vector Laboratories) followed by streptavidin-Alexa 543 (Molecular Probes). DNA was counterstained with DAPI (1 μg/ml) in Vectashield (Vector Laboratories). For dual protein/nucleic acid localization experiments, slides were first subjected to immunofluorescence, then postfixed in 4% formaldehyde/PBS followed by RNA- or DNA-FISH.

Microscopy

Nuclei were routinely examined using a Nikon Eclipse E800i epifluorescence microscope, with images collected using a Photometrics Coolsnap ES Mono digital camera. The images were pseudocolored, merged, and processed using Adobe Photoshop (Adobe Systems). Multiphoton optical-section stacks were collected using a Zeiss LSM 510 Meta microscope. Single optical sections using 40× averaging were acquired by simultaneous scanning to avoid artifactual shift between two optical channels. The 488 nm line of an argon laser was used for detection of FITC FLAG-tagged proteins, and the 543 nm line of a helium-neon laser was used for detection of Alexa 543 siRNA signals. For the detection of DAPI, either a 715 or 750 nm multiphoton tuned titanium-sapphire laser was used. Projections of 3D data stacks were composed using Imaris 4.1 software from Bitplane (http://www.bitplane.com).

Supplemental Data

Supplemental Data include three figures and six tables and can be found with this article online at http://www.cell.com/cgi/content/full/126/1/79/DC1/.

ACKNOWLEDGMENTS

O.P. performed all microscopy, P.C.N. generated siRNA blots, T.R. performed DNA methylation assays, and J.H. generated epitope-tagged Pol IV lines and coIP data. YFP-RDR2 and FLAG-DCL3 lines were generated by O.P. and A.V., respectively; C.S.P. wrote the manuscript. C.F.L. and S.E.J. generated the Myc-AGO4 transgenic line and contributed Figure 4B. O.P. and P.C.N. were supported by fellowships SFRH/BPD/17508/2004 and SFRH/BD/6520/2001, respectively, from the Fundação para a Ciência e Tecnologia (Portugal). Pikaard lab work was supported by NIH grants R01GM60380 and R01GM077590 and the Monsanto Company/Washington University Biology Research Agreement. C.F.L. was supported by Ruth L. Kirschstein National Research Service Award GM07185. S.E.J. is a Howard Hughes Medical

Institute Investigator. Work in the Jacobsen laboratory was supported by NIH grant GM60398. Any opinions, findings, and conclusions expressed in this material are those of the authors and do not necessarily reflect the views of NIH, HHMI, or the Monsanto Company. We thank Howard Berg (Donald Danforth Plant Science Center) for multiphoton microscopy training, Tom Juehne and Keming Song (Sigma-Aldrich Company) for Pol IV antibody production, Dr. Wanda Viegas (Instituto Superior de Agronomia, Portugal) for comentoring P.C.N., and Eric Richards (Washington University) for suggestions to improve the manuscript.

Received: March 1, 2006
Revised: March 31, 2006
Accepted: May 17, 2006
Published: July 13, 2006

REFERENCES

Almeida, R., and Allshire, R.C. (2005). RNA silencing and genome regulation. Trends Cell Biol. *15*, 251–258.

Aufsatz, W., Mette, M.F., van der Winden, J., Matzke, A.J., and Matzke, M. (2002). RNA-directed DNA methylation in Arabidopsis. Proc. Natl. Acad. Sci. USA *99*, 16499–16506.

Baulcombe, D. (2004). RNA silencing in plants. Nature *431*, 356–363.

Baumberger, N., and Baulcombe, D.C. (2005). Arabidopsis ARGONAUTE1 is an RNA Slicer that selectively recruits microRNAs and short interfering RNAs. Proc. Natl. Acad. Sci. USA *102*, 11928–11933.

Bernstein, E., Caudy, A.A., Hammond, S.M., and Hannon, G.J. (2001). Role for a bidentate ribonuclease in the initiation step of RNA interference. Nature *409*, 363–366.

Bertrand, E., Houser-Scott, F., Kendall, A., Singer, R.H., and Engelke, D.R. (1998). Nucleolar localization of early tRNA processing. Genes Dev. *12*, 2463–2468.

Boudonck, K., Dolan, L., and Shaw, P.J. (1999). The movement of coiled bodies visualized in living plant cells by the green fluorescent protein. Mol. Biol. Cell *10*, 2297–2307.

Buhler, M., Mohn, F., Stalder, L., and Muhlemann, O. (2005). Transcriptional silencing of nonsense codon-containing immunoglobulin minigenes. Mol. Cell *18*, 307–317.

Cao, X., Aufsatz, W., Zilberman, D., Mette, M.F., Huang, M.S., Matzke, M., and Jacobsen, S.E. (2003). Role of the DRM and CMT3 methyltransferases in RNA-directed DNA methylation. Curr. Biol. *13*, 2212–2217.

Carmell, M.A., Xuan, Z., Zhang, M.Q., and Hannon, G.J. (2002). The Argonaute family: tentacles that reach into RNAi, developmental control, stem cell maintenance, and tumorigenesis. Genes Dev. *16*, 2733–2742.

Cioce, M., and Lamond, A.I. (2005). Cajal bodies: a long history of discovery. Annu. Rev. Cell Dev. Biol. *21*, 105–131.

Clough, S.J., and Bent, A.F. (1998). Floral dip: a simplified method for Agrobacterium-mediated transformation of Arabidopsis thaliana. Plant J. *16*, 735–743.

Earley, K.W., Haag, J.R., Pontes, O., Opper, K., Juehne, T., Song, K., and Pikaard, C.S. (2006). Gateway-compatible vectors for plant functional genomics and proteomics. Plant J. *45*, 616–629.

Filipowicz, W., and Pogacic, V. (2002). Biogenesis of small nucleolar ribonucleoproteins. Curr. Opin. Cell Biol. *14*, 319–327.

Gasciolli, V., Mallory, A.C., Bartel, D.P., and Vaucheret, H. (2005). Partially redundant functions of Arabidopsis DICER-like enzymes and a role for DCL4 in producing trans-acting siRNAs. Curr. Biol. *15*, 1494–1500.

Grewal, S.I., and Rice, J.C. (2004). Regulation of heterochromatin by histone methylation and small RNAs. Curr. Opin. Cell Biol. *16*, 230–238.

Hannon, G.J. (2002). RNA interference. Nature *418*, 244–251.

Herr, A.J., Jensen, M.B., Dalmay, T., and Baulcombe, D.C. (2005). RNA polymerase IV directs silencing of endogenous DNA. Science *308*, 118–120.

Highett, M.I., Beven, A.F., and Shaw, P.J. (1993). Localization of 5 S genes and transcripts in Pisum sativum nuclei. J. Cell Sci. *105*, 1151–1158.

Kanno, T., Mette, M.F., Kreil, D.P., Aufsatz, W., Matzke, M., and Matzke, A.J. (2004). Involvement of putative SNF2 chromatin remodeling protein DRD1 in RNA-directed DNA methylation. Curr. Biol. *14*, 801–805.

Kanno, T., Huettel, B., Mette, M.F., Aufsatz, W., Jaligot, E., Daxinger, L., Kreil, D.P., Matzke, M., and Matzke, A.J. (2005). Atypical RNA polymerase subunits required for RNA-directed DNA methylation. Nat. Genet. *37*, 761–765.

Kiss, T. (2002). Small nucleolar RNAs: an abundant group of noncoding RNAs with diverse cellular functions. Cell *109*, 145–148.

Krogh, B.O., and Symington, L.S. (2004). Recombination proteins in yeast. Annu. Rev. Genet. *38*, 233–271.

Li, C.F., Pontes, O., El-Shami, M., Henderson, I.R., Bernatavichute, Y.V., Chan, S.W.-L., Lagrange, T., Pikaard, C.S., and Jacobsen, S.E. (2006). An ARGONAUTE4-containing nuclear processing center colocalized with Cajal bodies in *Arabidopsis thaliana*. Cell *126*, this issue, 93–106.

Lippman, Z., May, B., Yordan, C., Singer, T., and Martienssen, R. (2003). Distinct mechanisms determine transposon inheritance and methylation via small interfering RNA and histone modification. PLoS Biol. *1*, E67.

Mette, M.F., Aufsatz, W., van der Winden, J., Matzke, M.A., and Matzke, A.J. (2000). Transcriptional silencing and promoter methylation triggered by double-stranded RNA. EMBO J. *19*, 5194–5201.

Onodera, Y., Haag, J.R., Ream, T., Costa Nunes, P., Pontes, O., and Pikaard, C.S. (2005). Plant nuclear RNA polymerase IV mediates siRNA and DNA methylation-dependent heterochromatin formation. Cell *120*, 613–622.

Pederson, T. (1998). The plurifunctional nucleolus. Nucleic Acids Res. *26*, 3871–3876.

Pendle, A.F., Clark, G.P., Boon, R., Lewandowska, D., Lam, Y.W., Andersen, J., Mann, M., Lamond, A.I., Brown, J.W., and Shaw, P.J. (2005). Proteomic analysis of the Arabidopsis nucleolus suggests novel nucleolar functions. Mol. Biol. Cell *16*, 260–269.

Pontes, O., Lawrence, R.J., Neves, N., Silva, M., Lee, J.H., Chen, Z.J., Viegas, W., and Pikaard, C.S. (2003). Natural variation in nucleolar dominance reveals the relationship between nucleolus organizer chromatin topology and rRNA gene transcription in Arabidopsis. Proc. Natl. Acad. Sci. USA *100*, 11418–11423.

Pontier, D., Yahubyan, G., Vega, D., Bulski, A., Saez-Vasquez, J., Hakimi, M.A., Lerbs-Mache, S., Colot, V., and Lagrange, T. (2005). Reinforcement of silencing at transposons and highly repeated sequences requires the concerted action of two distinct RNA polymerases IV in Arabidopsis. Genes Dev. *19*, 2030–2040.

Rountree, M.R., and Selker, E.U. (1997). DNA methylation inhibits elongation but not initiation of transcription in Neurospora crassa. Genes Dev. *11*, 2383–2395.

Song, J.J., Smith, S.K., Hannon, G.J., and Joshua-Tor, L. (2004). Crystal structure of Argonaute and its implications for RISC slicer activity. Science *305*, 1434–1437.

Sontheimer, E.J., and Carthew, R.W. (2004). Molecular biology. Argonaute journeys into the heart of RISC. Science *305*, 1409–1410.

Tomari, Y., and Zamore, P.D. (2005). Perspective: machines for RNAi. Genes Dev. *19*, 517–529.

Vaucheret, H. (2005). RNA polymerase IV and transcriptional silencing. Nat. Genet. *37*, 659–660.

Verdel, A., Jia, S., Gerber, S., Sugiyama, T., Gygi, S., Grewal, S.I., and Moazed, D. (2004). RNAi-mediated targeting of heterochromatin by the RITS complex. Science *303*, 672–676.

Volpe, T.A., Kidner, C., Hall, I.M., Teng, G., Grewal, S.I., and Martienssen, R.A. (2002). Regulation of heterochromatic silencing and histone H3 lysine-9 methylation by RNAi. Science *297*, 1833–1837.

Wassenegger, M. (2005). The role of the RNAi machinery in heterochromatin formation. Cell *122*, 13–16.

Wassenegger, M., and Krczal, G. (2006). Nomenclature and functions of RNA-directed RNA polymerases. Trends Plant Sci. *11*, 142–151.

Xie, Z., Johansen, L.K., Gustafson, A.M., Kasschau, K.D., Lellis, A.D., Zilberman, D., Jacobsen, S.E., and Carrington, J.C. (2004). Genetic and functional diversification of small RNA pathways in plants. PLoS Biol. *2*, E104.

Zilberman, D., Cao, X., and Jacobsen, S.E. (2003). ARGONAUTE4 control of locus-specific siRNA accumulation and DNA and histone methylation. Science *299*, 716–719.

Zilberman, D., Cao, X., Johansen, L.K., Xie, Z., Carrington, J.C., and Jacobsen, S.E. (2004). Role of Arabidopsis ARGONAUTE4 in RNA-directed DNA methylation triggered by inverted repeats. Curr. Biol. *14*, 1214–1220.